Novel catalyst configuration to boost the yield of longer hydrocarbons from methanol-mediated CO<inf>2</inf> hydrogenation

N.B. When citing this work, cite the original published paper.
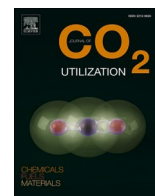
(article starts on next page)

Novel catalyst configuration to boost the yield of longer hydrocarbons from methanol-mediated CO_2 hydrogenation

Poonam Sharma, Phuoc Hoang Ho, Wei Di, Derek Creaser, Louise Olsson[*]

Chemical Engineering, Competence Centre for Catalysis, Chalmers University of Technology, SE-412 96 Gothenburg, Sweden
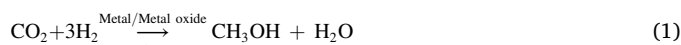
ABSTRACT

Various C_1 feedstocks and lower hydrocarbons (C_2-C_4) can be produced from CO_2 hydrogenation, which is an important way to utilize excess CO_2 and provide alternative fuel options for dwindling fossil fuels. Herein, a novel two-bed catalytic system was developed to increase the yield of liquid range hydrocarbons, where the first catalytic bed was composed of In_2O_3-ZrO_2 (13 wt. In %)/HZSM-5 and the second bed was a desilicated HZSM-5 placed downstream from the first bed. A maximum hydrocarbon selectivity was found to be about 86% with 7.2% CO_2 conversion at 533 K, while conversion increased up to 19.3% with 71.2% hydrocarbon selectivity at 623 K while keeping the pressure at 4.0 MPa. The selectivity of longer liquid range hydrocarbons (C_8-C_{12}) was increased from 29.2% to 42.4% using the oligomerization process in which the produced lower olefins from the first bed were oligomerized to enhance the liquid range hydrocarbon over desilicated HZSM-5. Additionally, a comparative study was carried out to examine the effect of desilication over HZSM-5 having different silica-to-alumina ratios of 24 and 59. Moreover, detailed characterizations were carried out before and after the desilication of the HZSM-5 to correlate catalytic activities with physical and chemical properties of the catalysts. The results suggest that a two-bed catalytic system is a promising option to increase the yield of liquid range hydrocarbons from methanol-mediated CO_2 hydrogenation while there was a negligible effect on CO_2 conversion due to the second bed.

1. Introduction

Carbon capture and utilization (CCU) is an important technique to solve various issues related to energy and global warming [1–3]. Surplus CO_2 which is the cause of global warming, could be a feedstock for value-added chemicals and fuels [4–6]. The CO_2 could be captured from the air or industry flue gases (cement, heat and power generation, chemical, etc.)[7]. Although, negative CO_2 emissions can only be achieved if CCU technology uses biogenic CO_2 [8]. Thus, many technologies based on photochemistry, electrochemistry, biochemistry, plasma chemistry, and solar thermochemistry have emerged to convert CO_2 into valuable chemical products [9,10]. In this context, CO_2 hydrogenation into fuels is highly desirable to reduce our dependence on fossil resources and mitigate global warming [11–14]. Hydrogen which is the second most important reagent for CO_2 hydrogenation, can be produced from renewable and sustainable energy resources [15,16].

The high global demand for liquid fuels [17,18] in combination with the huge problems with global warming makes it essential to develop new methods for renewable liquid fuel production. Methanol to gasoline

(MTG) synthesis offers a path to form liquid fuel where methanol could be produced from CO_2 hydrogenation [19]. The entire process involves two independent catalysts in two different steps as shown in Eqs. (1) and (2)[19].

$$CO_2 + 3H_2 \xrightleftharpoons{\text{Metal/Metal oxide}} CH_3OH + H_2O \qquad (1)$$

$$nCH_3OH \xrightarrow{\text{Zeolite}} n(CH_2) + nH_2O \qquad (2)$$

Generally, a modified Fischer-Tropsch Synthesis (FTS) process is used to prepare hydrocarbons directly from CO_2 where two main consecutive reactions occur [20,21]. The consecutive reactions include CO formation and the further conversion of CO to hydrocarbons via Fischer-Tropsch reactions. However, the selectivity of the liquid range hydrocarbons normally follows the Anderson-Schulz-Flory (ASF) distribution, which limits the selectivity for liquid range hydrocarbons, with a high fraction of CH_4. Recently, a new single-step process has been developed to produce hydrocarbons like lower olefins, aromatics and gasoline range hydrocarbons, directly from CO_2 hydrogenation over

bifunctional catalysts which is a combination of a CO_2 to methanol catalyst and a methanol to hydrocarbon catalyst [19]. A summary of reported studies in this area can be found in Table S1, Supplementary Information (SI). The product distribution is found to deviate from the ASF distribution in this process [22]. Single-step CO_2 hydrogenation could be an efficient method to increase the CO_2 conversion in the methanol synthesis step by its immediate conversion over the zeolite catalyst for the hydrocarbon synthesis [19]. Most studies use a composite of In_2O_3-ZrO_2 and zeolite to make a bifunctional catalyst and higher selectivities are reported towards lower olefins/paraffins ($C_2^=$-$C_4^=$ and $C_2 - C_4$ products account for 80–90% of hydrocarbons) from the CO_2 hydrogenation, as it is a challenging task to make longer chain hydrocarbons due to extreme inertness of the CO_2 molecule and high energy barriers for C-C coupling [19,23,24]. Previous works have shown that In_2O_3 is an effective catalyst for producing methanol by CO_2 hydrogenation, where oxygen vacancies have been suggested to be important [25]. The produced methanol can be converted into hydrocarbons by the acidic sites in the zeolite. Sun et al. developed a bifunctional catalyst, composed of In_2O_3 and HZSM-5 which was found to be highly selective for C_{5+} hydrocarbons [26]. The crystal size as well as the porosity of the catalyst could be a limiting factor for the synthesis of liquid-range hydrocarbons [27]. There are various applications for longer hydrocarbons, such as in the jet-fuel range (C_8-C_{16}) [28]. Therefore, further efforts are needed to increase the selectivity of liquid-range hydrocarbons and increase the selectivity for longer hydrocarbons.

There are different methods such as isomerization, cyclization, and oligomerization which can be employed to form liquid range hydrocarbons from lower hydrocarbons [29]. The catalytic oligomerization of lower olefins is an important method to obtain liquid-range hydrocarbons, whereas the lower olefins could be derived from various feedstock chemicals like methanol, ethanol and mixtures of hydrocarbons [30–32]. The oligomerization of light olefins over heterogenous catalysts depends on several variables, for example, the nature of the active sites and the textural properties of the catalysts [30,33]. The activity and stability of oligomerization catalysts are to a large extent affected by mass transfer (diffusion). Therefore, the utilization of macro- or mesoporous catalysts can be employed as a solution to surpass these diffusion limitations [34]. Zeolites were found to be good catalysts for oligomerization where macro- or mesoporosity can be created using a desilication process [34–36].

The overall goal is to produce longer hydrocarbons in the liquid range (C_8 to C_{12} hydrocarbons) from CO_2 hydrogenation. Therefore, the methanol-mediated CO_2 to hydrocarbons process is investigated, in which multiple catalytic processes are in synergy to generate liquid hydrocarbons in a single step. Herein, a novel two-bed configuration was developed to increase the selectivity for liquid hydrocarbons which can be used as fuel (C_{8+}) [28]. We have therefore combined the CTH (CO_2 to Hydrocarbons) process with oligomerization to increase the fraction of longer liquid range hydrocarbons. There are various reports where this process was separately used for the oligomerization of ethylene, propylene, butene and hexene over modified zeolites [37,38]. However, according to our knowledge, this is the first study where a bifunctional catalyst was combined with an oligomerization catalyst in a two-bed configuration for the synthesis of longer liquid fuel range hydrocarbons. In_2O_3-ZrO_2/HZSM-5 was used as the bifunctional catalyst while desilicated-HZSM-5 was employed as the oligomerization catalyst. The selectivity of liquid range hydrocarbons (C_8-C_{12}) increased from 29% to 42.5% over two-bed configurations. The changes in morphology, texture properties, crystallinity, thermal stability and acid strength of HZSM-5 and desilicated HZSM-5 are characterized and discussed in detail. In essence, this study explores catalyst modifications and process parameter optimization to advance knowledge regarding the CO_2 to hydrocarbon process, and more specifically with the aim to improve yields of hydrocarbons in the liquid range.

2. Experimental section

2.1. Catalyst preparation

ZrO_2 (monoclinic phase, extrudates, SZ 31164, NORPRO), In $(NO_3)_3 \cdot xH_2O$ (Indium nitrate, Alfa Aesar, 99.99%), and HZSM-5 (Akzo Nobel) with two different silica to alumina molar ratios (SiO_2/Al_2O_3, SAR = 27 and 57) were used. ZrO_2-supported In_2O_3 was prepared using an incipient wetness-impregnation method where $In(NO_3)_3 \cdot xH_2O$ salt was dissolved in a mixture of ethanol and deionized water and dropped directly onto the ZrO_2 powder. An indium amount corresponding to 13 wt% loading of In on ZrO_2 was used. The impregnated slurry was dried overnight at 333 K and calcined in air at 573 K for 3 h. Further, the dried powder was pressed, crushed, and sieved into granules to obtain granule sizes of $250 - 500$ μm. Ethanol, carborundum (SiC) and other solvents were purchased commercially.

Both HZSM-5, with different SARs, were desilicated using an alkaline solution of NaOH. Before the desilication process, the NH_4-ZSM-5 was calcined at 823 K for 5.5 h to form HZSM-5. Thereafter, the HZSM-5 was modified using a desilication process where the HZSM-5 (5 g) was mixed into 500 mL of a NaOH (0.2 M) solution and refluxed for 1.5 h at 338 K (Fig. 1)[37]. The refluxed solution was cooled and then filtered followed by washing with distilled water until pH 7 was reached. The washed sample was then dried in an oven at 373 K overnight. Further, the modified-ZSM-5 (3.5 g) was converted to NH_4-ZSM-5 by refluxing it in 70 mL of NH_4NO_3 solution (1 M) for 3 h and this ion-exchange treatment was repeated three times. The final sample was washed with distilled water and then the washed sample was dried in an oven at 373 K overnight. Further, the sample was calcined at 823 K for 5.5 h to obtain desilicated HZSM-5. The zeolite powders were pressed, crushed, and sieved to form granules sized 250–500 μm.

To prepare the bifunctional catalysts, the granules of In_2O_3 (13 wt% In)-ZrO_2 were mixed with equal-sized granules of HZSM-5 or desilicated HZSM-5 by shaking in a vessel in 1:1 mass ratio (Fig. S1, SI). The In loading on ZrO_2 was kept at 13 wt% in all catalytic reactions.

2.2. Catalyst characterization

The crystalline nature of the catalysts was examined using a powder X-Ray diffractometer (XRD). The experiments were conducted on a SIEMENS D5000 (Cu K_α radiation ($\lambda = 1.5$ Å), 40 mA and 45 kV, 2θ from 20° to 70° with a step size of 0.02°. The ^{27}Al and ^{29}Si magic angle spinning nuclear magnetic resonance (MAS NMR) experiments were carried out on a Bruker Avance III 500 MHZ magnet spectrometer equipped with a 4 mm double-resonance MAS probe. The ^{27}Al MAS NMR single pulse spectra were recorded at 130.3 MHz with a MAS spinning rate of 11 kHz. The single pulse ^{29}Si MAS NMR spectra with high power decoupling spectra (hpdec) were acquired at 99.4 MHz with a MAS spinning rate of 11 kHz. All chemical shifts were referenced externally to the methylene $(-CH_2-)$ group of adamantane set to 38.48 ppm (with sr =0).

The specific surface area, pore volume, and pore area of the catalysts were determined by N_2 sorption (Micromeritics Tristar 3000) at 77 K using the Brunauer–Emmett–Teller (BET) method. The catalysts (approximately 0.08 g) were outgassed in a N_2 flow at 498 K overnight before the measurements. Microporous and external surface areas were determined by the t-plot method whereas total pore volume (V_{total}) was determined by a single point at $p/p° = 0.97$.

The morphology of catalysts was determined using TEM (Titan 80–300, FEI Company, 300 kV). The sample was prepared by crushing the sample between two glass slides and dispersing it over a perforated carbon Cu grid.

The SAR ratios of the HZSM samples were examined using a Wavelength Dispersive X-ray Fluorescence (WDXRF) spectrometer with an Rh source at 60 kV and 125 mA.

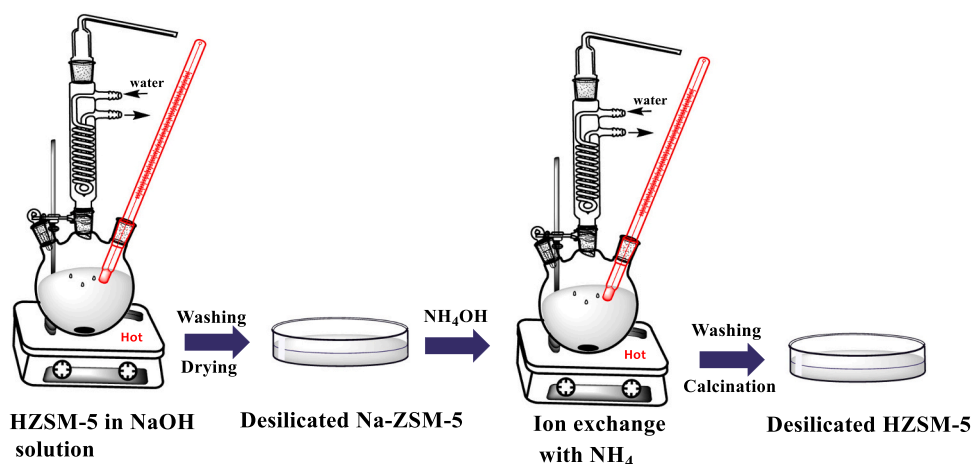The oxidation state was investigated using X-ray photoelectron

Fig. 1. Desilication process of HZSM-5.

spectroscopy (XPS) with a Physical Electronics (PHI) 5000 VersaProbe III Scanning XPS Microprobe. Focused monochromatic Al-Kα radiation was used with 1486.6 eV and C1s = 284.6 eV. The beam size was around 100 μm.

The strength and number of acid sites of the catalysts were studied using ammonia-temperature programmed desorption (NH₃-TPD). The powder catalysts (30 mg) were loaded into a microreactor and pre-treated in a flow of pure Ar at 673 K for 1 h prior to the experiment. Thereafter, the microreactor was cooled to 373 K when flushing the sample with Ar and the catalyst was then exposed to NH₃ (2000 ppm in Ar) for 1.5 h with a flow rate of 20 NmL/min. This was followed by purging the sample with Ar for 1 h at 373 K to remove the physisorbed NH₃ on the sample surface. Finally, the desorption behavior was studied by increasing the temperature up to 973 K with a ramp rate of 10 K/min. The concentration of NH₃ gas in the outlet stream was continuously monitored using a mass spectrometer (HIDEN, HPR-20 QUI, m/z = 17).

Thermogravimetric analysis (TGA) was carried out to examine the thermal stability and the effect of desilication (TGA/DSC3 +, Mettler Toledo). HZSM-5 pellets were heated from 308 to 1073 at 5 K/min in a flow of 75 NmL/min of N₂ to check the stability of fresh HZSM-5/ desilicated HZSM-5 whereas air is used for spent desilicated HZSM-5.

2.3. Catalytic tests

The activity of the catalysts was examined in a high-pressure fixed bed reactor (VINCI Technologies, France), where the tubular stainless-steel reactor was positioned vertically. The two processes were performed in this continuous reactor: (1) CO₂ hydrogenation to form methanol and (ii) methanol conversion to hydrocarbons (MTH). In our earlier study [39], the activity of In₂O₃ -ZrO₂ was examined for methanol synthesis at various temperatures and pressure to determine a suitable temperature and pressure for the reaction. 0.5 g of the In₂O₃-ZrO₂ was packed into the reactor in such a way that the catalyst bed was in contact with a thermocouple tip to measure the bed temperature during the reaction. The catalyst bed was held between two thin layers of quartz wool and had a depth of 0.7 cm. It was situated at about the centre vertical position of the 21.5 cm long reactor tube (inner diameter 12.7 mm). The remaining up- and downstream portions of the reactor tube were filled with SiC (500 μm size). Further, the reactor was placed inside a furnace and connected to gas lines. The flows of the gases (Ar, CO₂ and H₂) were controlled via separate mass flow controllers upstream of the reactor. Prior to the reaction, the catalyst was pre-treated at 573 K in Ar (30 NmL min⁻¹) for 1 h at atmospheric pressure. The reactor was then cooled down to the reaction temperature and thereafter the feed gas was switched to CO₂ and H₂ and the pressure was changed to the final total pressure. Reaction conditions were as

follows: H₂/CO₂ = 3 (molar feed ratio), the temperature varied from 493 to 573 K and the gauge pressure ranged from 3.0 to 4.0 MPa. Data were collected for 8 h at each temperature.

Further, the bifunctional catalysts were prepared by mixing In₂O₃-ZrO₂ with zeolite HZSM-5 and they were tested at various temperature ranges to form hydrocarbons from the CO₂. In this context, the catalysts were tested using three configurations (A, B, and C) inside the reactor, which are shown in Fig. 2. Briefly, configuration A consists of one bed with physically mixed In₂O₃-ZrO₂/HZSM-5, configuration B consists of two beds the first with mixed In₂O₃-ZrO₂/HZSM-5 followed downstream by a second bed of desilicated-HZSM-5 and finally, and configuration C consists of one bed of physically mixed In₂O₃-ZrO₂/desilicated-HZSM-5. In configurations A and C, a total of 1.0 g of composite catalyst (the mass of In₂O₃-ZrO₂ to HZSM-5 was 1:1) was packed inside the reactor using the method described above. In configuration B, 0.5 g of desilicated-HZSM-5 was placed downstream from the 1.0 g of mixed In₂O₃-ZrO₂/ HZSM-5 as used in configuration A. The catalyst beds were separated by a layer of SiC (1.0 g) and a thin layer of quartz wool was placed up and downstream of both catalyst beds to ensure that each of the catalysts was separated from SiC. The position of the upstream bed was about the same inside the reactor in configurations A, B and C. In configurations A and C, the same amount of SiC was used to keep the upstream catalyst bed position the same inside the reactor, while in configuration B, the amount of downstream SiC was adjusted accordingly to obtain the same position of the upstream catalyst bed. The thermocouple tip was always in contact with the upstream bed.

In all cases, tests were conducted at temperatures ranging from 553 to 623 K, gauge pressures from 3.0 to 4.0 MPa, and with a H₂:CO₂ feed molar ratio of 3:1. It was found that a high yield of methanol could be achieved at 553 K and 3.0 MPa over the In₂O₃-ZrO₂ catalyst alone with
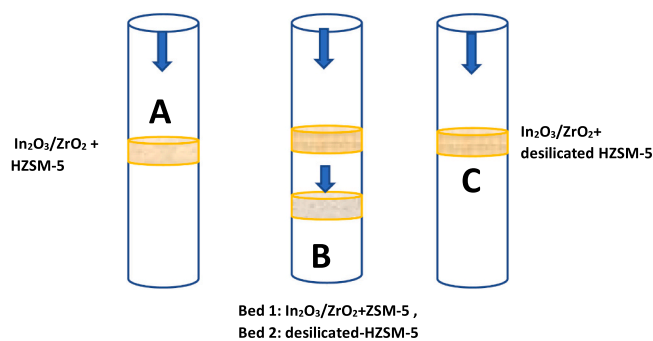

Fig. 2. Bed configurations inside the reactor (A) In₂O₃-ZrO₂/HZSM-5, (B) In₂O₃-ZrO₂/HZSM-5 + desilicated-HZSM-5, and (C) In₂O₃-ZrO₂/desilicated-HZSM-5. Arrows indicate the gas flow direction through the reactor.

satisfactory CO_2 conversion. Therefore, this temperature and pressure were selected as a starting reaction temperature and pressure for the hydrocarbon synthesis with the bifunctional catalysts. Also according to the literature, a suitable temperature range for MTH over HZSM-5 is typically from 623 to 823 K,[40] thus the studied temperature range here for CTH was extended up to 623 K.

The outlet streams of the gaseous products were analyzed using an on-line gas chromatograph (GC, SCION 456) equipped with a thermal conductivity (TCD) and a flame ionization detector (FID). The product samples were separated using HS-Q (80/100) and HP- Al/S (30 *0.53 mm, 15 μm) packed columns (Agilent Technologies, Inc.). The quantification and identification of the product stream were done based on calibration standards of known concentrations of different components. It should be noted that due to limitations in the GC column it was not possible to differentiate between alkanes, alkenes and aromatics for longer hydrocarbons. The same calibration factor was used for hydrocarbons and their corresponding branched isomers. An effective carbon number calibration factor was used for the closest carbon number compounds. Individual and higher aliphatic products were lumped together based on their retention times using the calibration of standard mixtures. Based on the standard solutions, peaks with retention times of up to 12 min were associated with C_2-C_5 hydrocarbons. Peaks between 12 and 19 min were related to C_6-C_8 hydrocarbons, while peaks beyond this range were considered as C_{9+} hydrocarbons. Examples of GC spectra are added in the Supplementary material, Fig. S2. For each set of conditions, samples were taken throughout 2–3 h to ensure that the final reported results are for steady-state operation. CO_2 conversion, product selectivities and hydrocarbon distributions were calculated based on the molar flow rates according to the following equations:

$$XCO2 = \frac{F_{CO2,in} - F_{CO2,out}}{FCO2, in} \times 100\%$$

$$SCH3OH = \frac{F_{CH3OH,out}}{F_{CO2,in} - F_{CO2,out}} \times 100\%$$

$$SCO = \frac{F_{CO,out}}{F_{CO2,in} - F_{CO2,out}} \times 100\%$$

$$SHC = \frac{\sum_n nF_{CnHm,out}}{F_{CO2,in} - F_{CO2,out}} \times 100\%$$

$$DHC = \frac{nF_{CnHm,out}}{\sum_n nF_{CnHm,out}} \times 100\%$$

Where $F_{CO2,in}$ and $F_{CO2,out}$ are the CO_2 molar flow rates at the inlet and outlet, respectively. $F_{CH3OH,out}, F_{CO,out}$ and $F_{CnHm,out}$ denotes the molar flow rates of methanol, CO, and a certain hydrocarbon (C_nH_m) product, respectively. It should be noted that there are two ways of expressing selectivity for hydrocarbon products, the hydrocarbon selectivity (S_{HC})

which is the percent of carbon from converted CO_2 that has formed the different hydrocarbon products and the hydrocarbon distribution (D_{HC}) which is the distribution of carbon among only the hydrocarbon products.

3. Results and Discussion

3.1. Catalyst characterization

In loading on ZrO_2 and SAR ratio in HZSM-5 were measured by WDXRF analysis. The measured In loading was 11.9 wt% which was close to the nominal value (13 wt% In). The SAR ratio in the commercial HZSM-5 with reported SAR = 27, was measured to be 24 before desilication which decreased to 21 upon desilication. The SAR ratio was measured to be 59 in the commercial HZSM-5 having a reported SAR = 57. After desilication, the SAR decreased to 18 for this sample (Table 1).

The crystallinity of the ZrO_2-supported In_2O_3 catalyst was studied using XRD analysis. The XRD for In_2O_3-ZrO_2 is reported in our earlier study [39] and it showed that the sample had characteristic diffractions of both In_2O_3 (PDF#65–3170)[41,42] and monoclinic ZrO_2. No other peaks were identified, which suggests that the In_2O_3-ZrO_2 exhibited good crystallinity.

The textural properties of the zeolites were examined using N_2 adsorption-desorption isotherms. Both the pristine HZSM-5 samples (SAR = 24 and SAR = 59) and desilicated zeolites show a typical characteristic of type I isotherm with pore fillings at very low relative pressures (p/p° < 0.05), confirming the microporous nature of the zeolite (Fig. 3) [43]. Additionally, a hysteresis of type H4 (close to p/p° = 0.45) was also observed during the desorption, suggesting the presence of mesopores in aggregated or hierarchical zeolites [44]. The hysteresis of the desilicated zeolite was wider than that of the parent zeolite, indicating the creation of more mesoporosity [45]. The specific surface area was found to be 359 and 429 m^2 g^{-1} for zeolites of SAR = 24 and SAR = 59, respectively (Fig. 3a). The micropores accounted for approximately 77% of the total specific surface area for the zeolite of SAR = 24 while this was 58% for the sample of SAR = 59. After desilication, the N_2 uptake was enhanced at a higher relative pressure for both the desilicated samples compared to their parent counterparts. The external surface area and mesopore volume of the desilicated SAR = 24 increased whereas the microporous surface area and pore volume decreased, indicating the generation of mesoporosity inside the framework (Table 1) [46]. The observation was different for HZSM-5 (SAR = 59) where the total surface area slightly decreased due to the loss of S_{micro} while $S_{external}$ increased after the desilication. The mesoporosity was also introduced due to the loss of microporosity in the study by Gil et al. [35]. It could be possible that the desilication of the framework may widen the micropores and some part of the desilicated Si blocked the micropores of the zeolite and this results in a slight loss in the micro

Table 1

Porous and compositional properties of HZSM-5 (SAR = 24 & SAR = 59) before and after desilication.

Catalysts	Porous properties							[f]Acidity	
	Measured (SAR ratio)[a]	$S_{BET}^{[b]}$ (m^2/g)	$S_{micro}^{[c]}$ (m^2/g)	$S_{external}^{[d]}$ (m^2/g)	$V_{micropore}^{[c]}$ (cm^3/g)	$V_{mesopore}^{[e]}$ (cm^3/g)	Average pore size[d] (Å)	T_{max} (K)	Total NH_3 desorbed (μmolg^{-1})
HZSM-5	24	359	275	84	0.133	0.072	55.6	446 664	803
Desilicated HZSM-5	21	378	259	119	0.126	0.159	50.8	455 679	1115
Spent Desilicated HZSM-5	21	327	184	143	0.089	0.176	53.7	–	-
HZSM-5	59	429	250	178	0.121	0.132	25.0	439 638	796
Desilicated HZSM-5	18	423	225	197	0.109	0.351	51.6	447 654	478

[a]Determined by XRF.[b]BET method.[c]t-plot method.[d]BJH method.[e]$V_{mesopore}$ = $V_{(pore\ at\ p/po\ =\ 0.97)}$ − $V_{micropore}$.[f]NH_3-TPD.
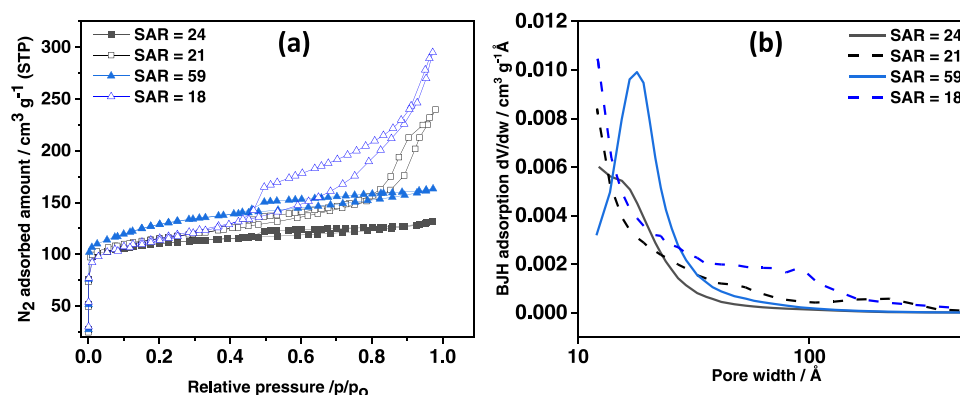
Fig. 3. N_2 adsorption-desorption isotherms of (a) HZSM-5 (SAR = 24), Desilicated-HZSM-5 (SAR = 21), HZSM-5 (SAR = 59) and, Desilicated HZSM-5 (SAR = 18), and (b) Calculated pore size distributions (from the adsorption branch), and Pore width distribution of HZSM-5 (SAR = 24), Desilicated-HZSM-5 (SAR = 21), HZSM-5 (SAR = 59) and, Desilicated-HZSM-5 (SAR = 18).

porous surface area for the desilicated HZSM-5 or that the zeolite structure is partly damaged due to loss of Al with Si [46], which indeed was observed during NMR of Si and Al atoms. In addition, the BET surface area of In_2O_3-ZrO_2 was found to be 60 m^2g^{-1} with 0.21 cm^3g^{-1} in pore volume which was reported in our earlier study [39].

To examine the effect of desilication on the crystallinity of HZSM-5, XRD analysis was carried out before and after the desilication of HZSM-5. The diffraction patterns of HZSM-5 (SAR = 24 and SAR = 59), and the resulting desilicated HZSM-5 (SAR = 21 and SAR = 18) are shown in Fig. 4. The original HZSM-5 samples with SAR of 24 and 59 resulted in highly crystalline diffraction patterns whereas a decrease in peak intensity was observed after the desilication [37]. The desilication process results in the removal of Si from the framework, which causes a partial disordering of the structural arrangement and a decreased SiO_2/Al_2O_3 ratio. It was observed that the desilication was higher for SAR = 59 than SAR = 24 which has also been observed in earlier studies [37,47]. Thus,

the HZSM-5 sample with SAR = 59 lost more crystallinity than SAR = 24 after desilication, as evident from its larger decrease in peak intensity, as shown in Fig. 4b.

Further, to gain more information about the Si and Al environment after desilication, ^{29}Si and ^{27}Al MAS NMR spectra were collected and are presented in Figs. 4c and 4d, respectively. The results clearly indicate that the HZSM-5 samples underwent varying degrees of desilication accompanied by dealumination. Two distinct resonance peaks were observed at approximately − 112 ppm and − 105 ppm in the ^{29}Si MAS spectrum. The peak at − 110 ppm is typically associated with the Si atom in the Q4 (0Al) configuration, while the peak at around − 104 ppm can be assigned to Q4 (1Al) [48]. In the desilicated HZSM-5 sample with SAR of 24, the signal attributed to Q4(1Al, −104 ppm) appeared slightly weaker, whereas the Q4 (0Al) peak experienced a slight shift. This suggests that controlled desilication occurred in the SAR = 24 sample. In contrast, a severe desilication was observed in the desilicated HZSM-5
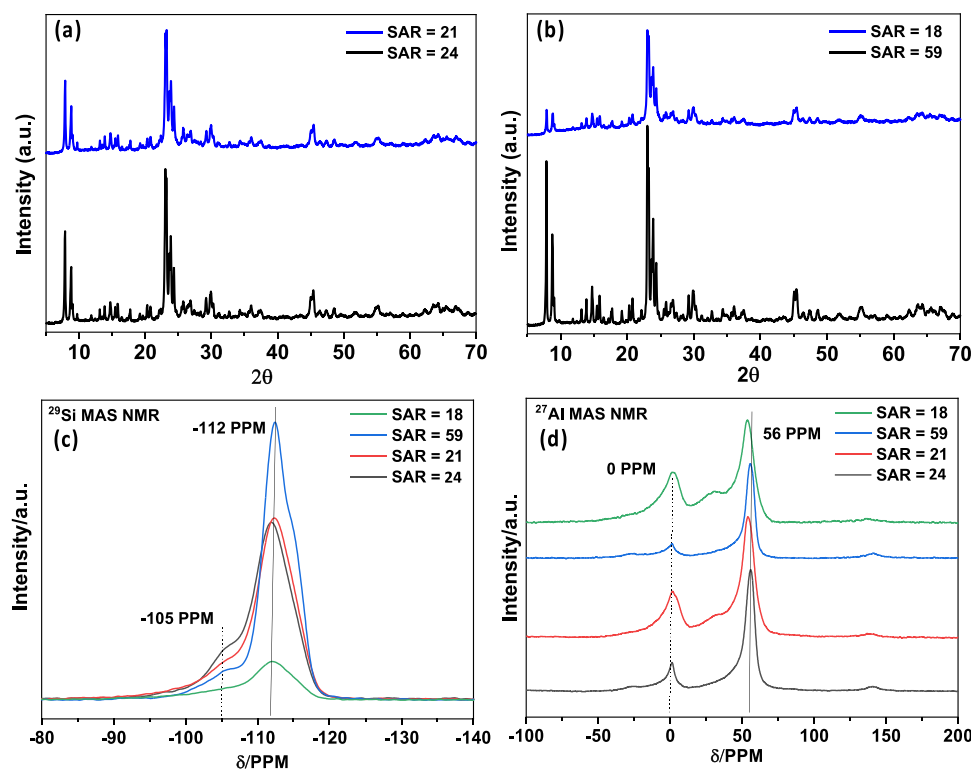

Fig. 4. XRD patterns of (a) HZSM-5 having SAR = 24 and SAR = 21 (b) HZSM-5 having SAR = 59 and SAR = 18, (c) ^{29}Si MAS NMR of ZSM-5 having SAR = 27, 21, 59 and 18, and (d) ^{27}Al MAS NMR of ZSM-5 having SAR = 27, 21, 59 and 18.

sample with a SAR of 59, as indicated by a drastic decrease in the intensity of signals related to both Si atoms (Fig. 4c).

Regarding the ^{27}Al NMR analysis of HZSM-5, two signals were observed at 60 ppm and 0 ppm (Fig. 4d), which can be assigned to tetrahedrally coordinated Al atoms and extra framework octahedrally coordinated Al atoms, respectively [48]. It was observed that the desilication process led to dealumination in both SARs, as the intensity of the peak related to extra framework alumina increased after desilication in SAR = 21 and SAR = 18. In conclusion, it can be inferred that controlled desilication occurred in the SAR = 24 sample, whereas a higher degree of desilication was observed in the SAR = 59 sample, resulting in framework loss. These findings align with the XRD analysis, which demonstrated more significant crystallinity loss in the SAR = 59 sample, while the zeolite framework was retained in the same (as shown in Fig. 4b).

The strength and number of acid sites were measured using NH$_3$-TPD (Table 1). The extraction of Si affects the number of acid sites as well as their strength [46]. NH$_3$-TPD measurements show two peaks for the HZSM-5 samples which can be assigned to weak (around 450 K) and strong (around 650 K) acid sites as shown in Fig. 5 [37]. Blank NH$_3$-TPD data (without sample) was used for baseline correction in the TPD plots, and the total acidities were estimated by integrating the corrected concentration of NH$_3$ desorbed per gram of HZSM-5.

The strength and number of acid sites, for both weak sites as well as strong sites, increased after desilication of the HZSM-5 from SAR = 24 to SAR = 21. The lower temperature peak was observed at 446 K and the higher temperature peak was at 664 K for HZSM-5 (SAR = 24), which further shifted to higher temperatures, of 455 K and 679 K after desilication, respectively. However, the high temperature peak before desilication is quite small which makes it difficult to determine the exact temperature for the maximum. Total NH$_3$ uptakes increased from 803 to 1115 μmol g^{-1} after desilication in case of HZSM-5 (SAR = 24). The slight shift to the higher temperature of the peaks after the desilication is possibly related to a change in the types/configurations of the acidic sites. A loss of silanol and formation of extra framework alumina could influence the strength of the weak acidic sites whereas the configuration of Si-O-Al-OH in the crystal fragments disintegrated from the zeolite structure could affect the strength of the strong acidic sites (high-temperature peaks). The number of strong acid sites (peak at high temperature) increased. Such increment in the strong acidity can related to the formation of abundant pieces of the crystal due to the desilication by NaOH giving a higher density of AlO$_4$ (due to a higher level of exposure) as reported recently by Cheng et al. [49].

It should be noted that the change in the amount of weak acid sites (peak at low temperatures) did not follow the same trend between the two desilicated samples. Moreover, for HZSM-5 (SAR = 59) there was an unexpected drop in ammonia uptake observed. The amount of NH$_3$ uptakes decreased from 796 to 478 μmolg^{-1} after desilication. However, the desorption peak at a high temperature (654 K) was still larger than that of the parent (SAR = 59) which was consistent with the increment of the strong Brønsted acid sites at lower Si/Al after the desilication [44]. The drop in the total NH$_3$ uptake could be related to a loss in total specific surface area (Table 1) for this sample. In addition, the high Si extraction from the framework of this sample which causes a greater amount of disorder to the zeolite structure and it is also possible that some sites are blocked by detached Si as well as by extra framework alumina due to loss of framework Al with Si (during desilication which results in loss of Si and Al) [46]. These observations are in good agreement with NMR and N$_2$ physisorption analysis.

To elucidate the effect of desilication on the morphology of the zeolites, transmission electron microscopy was used. The micrographs from both pristine and desilicated HZSM-5 are shown in Fig. 6. The TEM images of the pristine zeolite confirm the microporous structure with a relatively smooth surface which later transformed to a more course and irregular surface after desilication, which is consistent with the creation of mesopores due to Si extraction as indicated by the N$_2$ sorption analysis [37,50].

Fig. 7 shows the TGA curves of HZSM-5 and desilicated HZSM-5. It can be observed that the TGA profile of desilicated HZSM-5 is different from pristine HZSM-5. Up to 670 K a weight loss of 5.5% and 2.5% were detected for HZSM-5 (SAR = 24) and HZSM-5 (SAR = 59), respectively. These weight losses can be attributed to the desorption of matrix-absorbed water. A higher weight loss, i.e. larger amount of desorbed water, for the lower SAR sample is expected since it contains more Brønsted acid sites. The loss after desilication in the case of HZSM-5 (SAR = 24, 5.5–4.9%) was quite similar, although slightly less. For this sample the decrease in SAR ratio was quite small from 24 to 21, which could explain that the TGA was quite similar. However, for the HZSM-5 (SAR = 59) the desilicated sample (SAR=18) had a large increase in weight loss from 2.5% to 3.9%. This can be attributed to the disrupted structure and the increased hydrophilic nature of the desilicated HZSM-5 (SAR = 18), leading to an increased moisture content within the zeolite.

The In$_2$O$_3$-ZrO$_2$ was previously examined for methanol synthesis and detailed characterization of In$_2$O$_3$-ZrO$_2$ was presented in our earlier publication [39]. Briefly, we found three O1s peaks at 533.0, 531.0, and 529.7 eV, which we assigned to OH, oxygen defects and O$_{lattice}$, respectively. According to Martin et al. [25] the oxygen defects are suggested to be the active sites. Carbonate (CO$_3^{2-}$) and bicarbonate (HCO$_3^-$) species were observed on the surface of In$_2$O$_3$-ZrO$_2$ during the
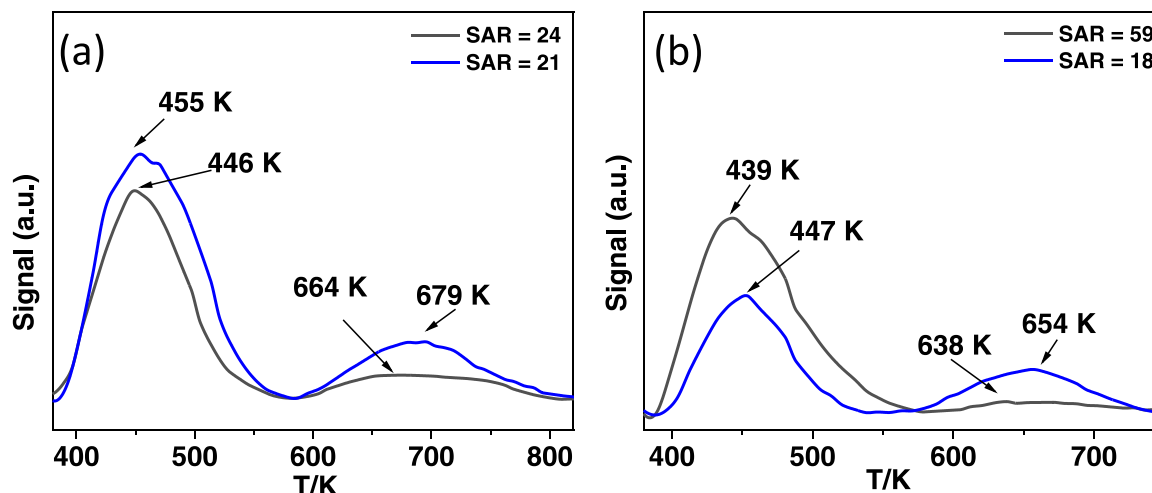

Fig. 5. NH$_3$-TPD of (a) HZSM-5 (SAR = 24) and, (b) HZSM-5 (SAR = 59) before and after desilication.
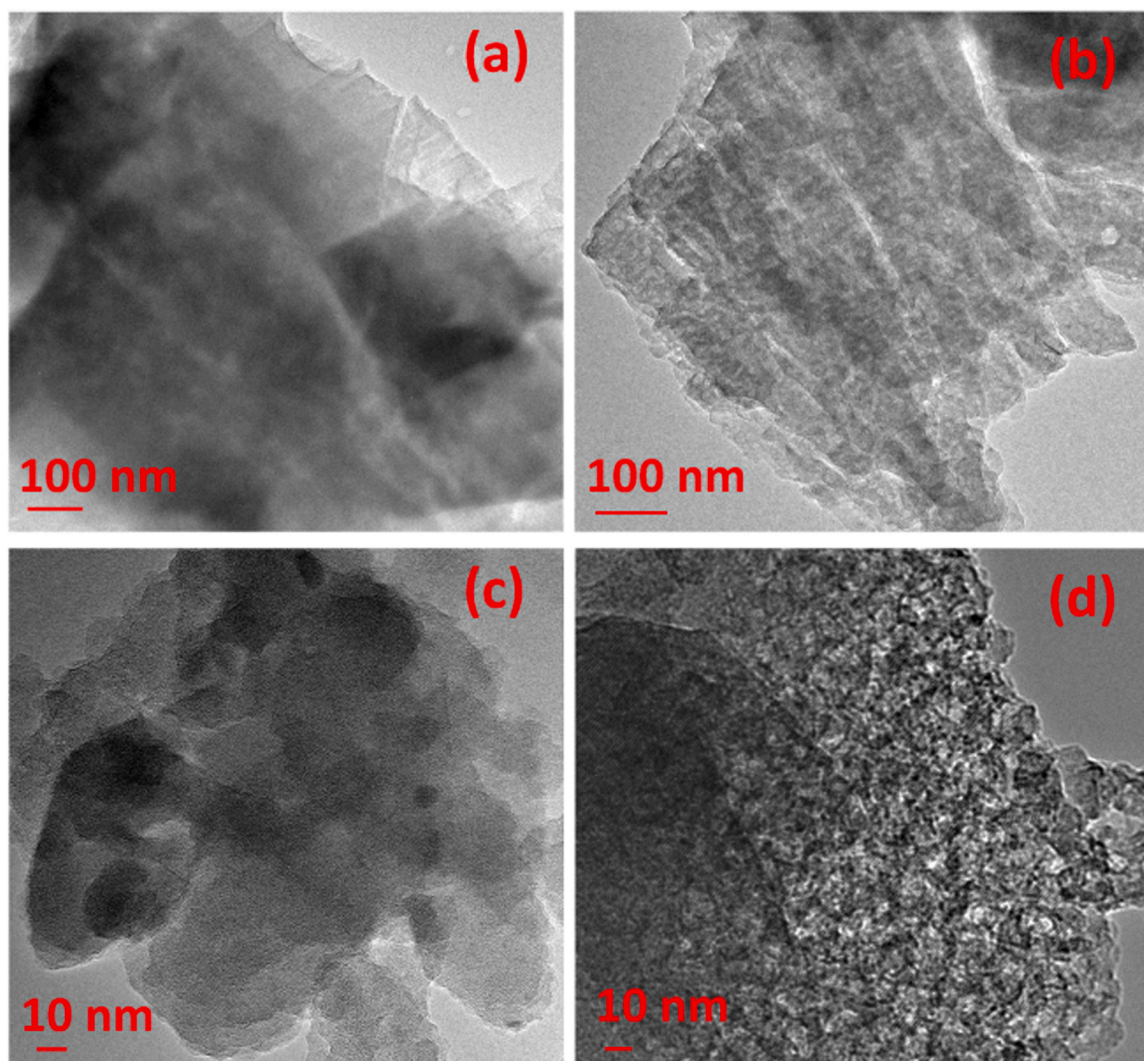
Fig. 6. TEM images of (a) HZSM-5 (SAR = 24), (b) Desilicated-HZSM-5 (SAR = 21), (c) HZSM-5 (SAR = 59), and (d) Desilicated-HZSM-5 (SAR = 18).
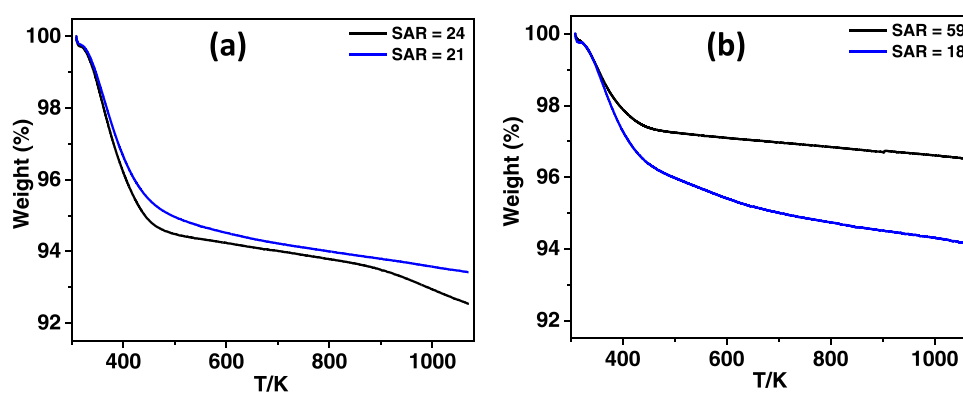

Fig. 7. TGA curves of (a) HZSM-5 (SAR = 24 and 21) and, (b) HZSM-5 (SAR = 59 and 18) before and after desilication.

in-situ DRIFT analysis. Moreover, the XRD patterns showed that In_2O_3-ZrO_2 had good crystallinity after preparation.

3.2. Catalytic activity results

3.2.1. CO₂ hydrogenation to methanol

The results for CO_2 hydrogenation over In_2O_3-ZrO_2 was shown in our

earlier paper [39]. We examined temperature from 493 to 573 K using $H_2/CO_2 = 3$ (feed molar ratio), and pressure at 3.0 MPa. Generally, with increasing temperature as the CO_2 conversion increased, the CO selectivity increased and CH_3OH selectivity decreased. Over the examined temperature range a reasonable compromise between CO_2 conversion and CH_3OH selectivity is found at 553 K, with 7.9% CO_2 conversion giving 74% CH_3OH and 26% CO selectivity. Therefore, this reaction

temperature was included in the temperature range when studying hydrocarbon synthesis in the current paper.

3.2.2. CO₂ to hydrocarbons via methanol over a bifunctional catalyst

Initially, In_2O_3-ZrO_2 was combined with a methanol to hydrocarbon (MTH) catalyst for the synthesis of hydrocarbons (HCs). HZSM-5 with SAR = 24 and SAR = 59 were used as the MTH catalysts. Further, the composite catalyst (In_2O_3-ZrO_2/HZSM-5) was tested at 3.0 and 4.0 MPa, at 553, 573, and 623 K to form hydrocarbons. The catalytic activity of each composite catalyst was tested in a sequence from low temperature to high temperature first at 3.0 MPa, and then the pressure was increased, and temperature decreased to 4.0 MPa and 553 K, respectively, before testing again the activity from low temperature to high temperature. Fig. 8 shows the results of configuration A in which In_2O_3-ZrO_2 and HZSM-5 (SAR = 24 and SAR = 59) were mixed in one bed. At 553 K, the HCs selectivity reached up to 81.3% with 14.8% CO selectivity at a CO_2 conversion of 6.9% at 3.0 MPa over In_2O_3-ZrO_2/HZSM-5 (SAR = 24, Fig. 8). The CO_2 conversion (7.4%) and HCs selectivity (83.2%) slightly increased when the pressure was increased to 4.0 MPa. Moreover, the CO_2 conversion was 17.2% with 60.2% HCs selectivity over configuration A (SAR = 24) at 623 K with pressure at 4.0 MPa.

The results were slightly different over the HZSM-5 with SAR = 59, where the conversion and HCs selectivity were slightly lower compared to HZSM-5 (SAR = 24) at 553 and 573 K, while the CO selectivity was somewhat higher. Higher CO_2 conversion and HCs selectivity over SAR = 24 may be due to more acid sites which can more quickly convert the CH_3OH to HCs. Since the formation of methanol is equilibrium limited, quicker conversion of methanol to HCs alleviates the equilibrium restriction and leads to higher CO_2 conversion and HCs selectivity. Surprisingly, the CO_2 conversion and HCs selectivity were higher over SAR = 59 than SAR = 24 at 623 K. This could be due to the higher acidity of SAR = 24, which leads to greater formation of HCs at lower temperatures, which might have caused some blockage of the active sites and hindered the formation of HCs at higher temperatures [51,52]. In addition, at higher temperatures it is possible that the RWGS became so dominant that the benefit of more acidic sites (SAR = 24) for the conversion of methanol was less important.

3.2.3. Increasing the fraction of longer hydrocarbons (C_8-C_{12}) using oligomerization process

The HCs were a combination of lower alkanes (C_2-C_4), lower olefins ($C_2^=$ – $C_4^=$), and C_{5+} HCs which includes aromatics. Since this study aims to increase the fraction of longer HCs, we developed a novel catalytic system using an oligomerization catalyst bed below the In_2O_3-ZrO_2/HZSM-5 bed to oligomerize the lower olefin fraction of HCs. As an oligomerization catalyst, desilicated-HZSM-5 was prepared (SAR = 21 and SAR = 18) by removing some of the Si inside the framework of HZSM-5 using an alkaline treatment that creates mesoporosity inside the framework. The desilicated HZSM-5 was found to have different crystallinities, texture properties and acid strength as described in Section 3.1.

In the oligomerization process, the desilicated-HZSM-5 was placed downstream from the In_2O_3-ZrO_2/HZSM-5 bed (Configuration B). The CO_2 conversion was found to be 7.2% with 68.0% C_{5+} selectivity at 553 K and 3.0 MPa when the desilicated HZSM-5 (SAR = 21) was placed downstream from In_2O_3-ZrO_2/HZSM-5 as a second bed (Fig. 9a). Further, the CO_2 conversion and C_{5+} selectivity changed to 19.3% and 30.1% at 623 K, respectively (See SI, Fig. S3). In addition, the CO_2 conversion and HCs selectivity increased up to 7.3% and 70.3% at 4.0 MPa, respectively (Fig. 9c). The oligomerization reactions are a sequence of acid-catalyzed-shape-selective polymerization and isomerization reactions over HZSM-5. The chemistry and mechanism of oligomerization over HZSM-5 have been studied in detail [36]. The CO_2 conversion was 6.7% with 69.1% C_{5+} selectivity when HZSM-5 having SAR = 18 was placed as a second bed (Fig. S4d, See SI). Further, the CO_2 conversion increased up to 19.3% and C_{5+} selectivity decreased to 46.0% at 623 K (Fig. S4f, See SI). The CO_2 conversion and selectivities of methanol/DME, CO, and HCs over configurations A, B, and C for the
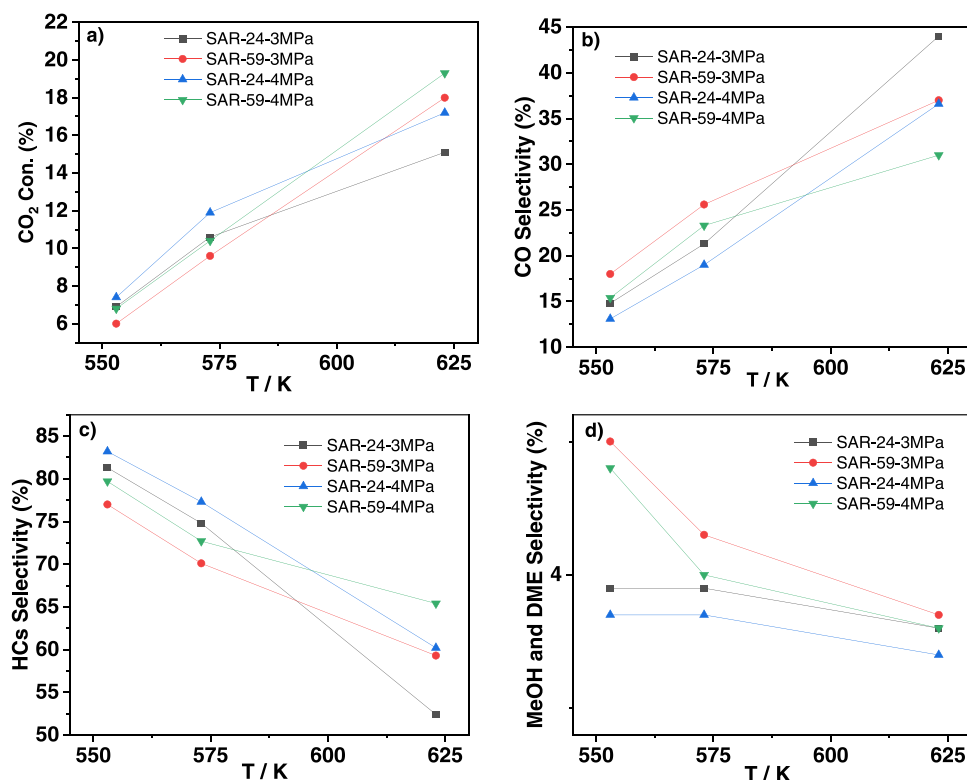

Fig. 8. Catalytic performance of In_2O_3-ZrO_2/HZSM-5 (Configuration A, with SAR = 24 & SAR = 59) at various temperatures and pressure at 3.0 and 4.0 MPa: (a) CO_2 conversion (b) CO selectivity (c) Hydrocarbons selectivity, and (d) Methanol and DME selectivity.
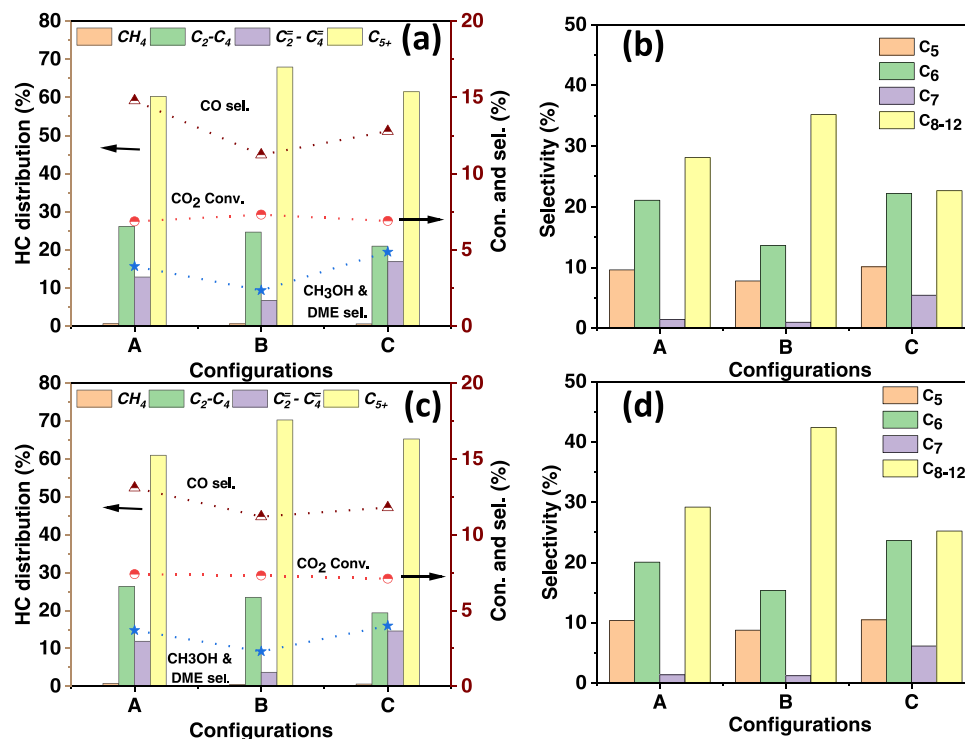
Fig. 9. CO_2 conversion, hydrocarbons distribution and selectivities over Configuration A, B, and C at 553 K (a & b) 3.0 MPa, and (c & d) 4.0 MPa. Configuration A: In_2O_3-ZrO_2/HZSM-5 (SAR = 24), Configuration B: In_2O_3-ZrO_2/HZSM-5 (SAR = 24) + desilicated-HZSM-5 (SAR = 21), and Configuration C: In_2O_3-ZrO_2/desilicated-HZSM-5 (SAR = 21).

remaining reaction conditions are shown in supporting information (Figs. S3 and S4). The selectivity for C_{5+} increased up to 70.3% among hydrocarbons at the expense of lower olefins ($C_2^=$ −$C_4^=$, Fig. 9c) as the selectivity of lower olefins (up to 5%) decreased after oligomerization at

553 K and 4.0 MPa. The intensity of oligomerization decreased with the increasing number of carbons in the olefin.

To examine the direct effect of the desilicated-HZSM-5 in hydrocarbon synthesis, a configuration (Configuration C) was examined
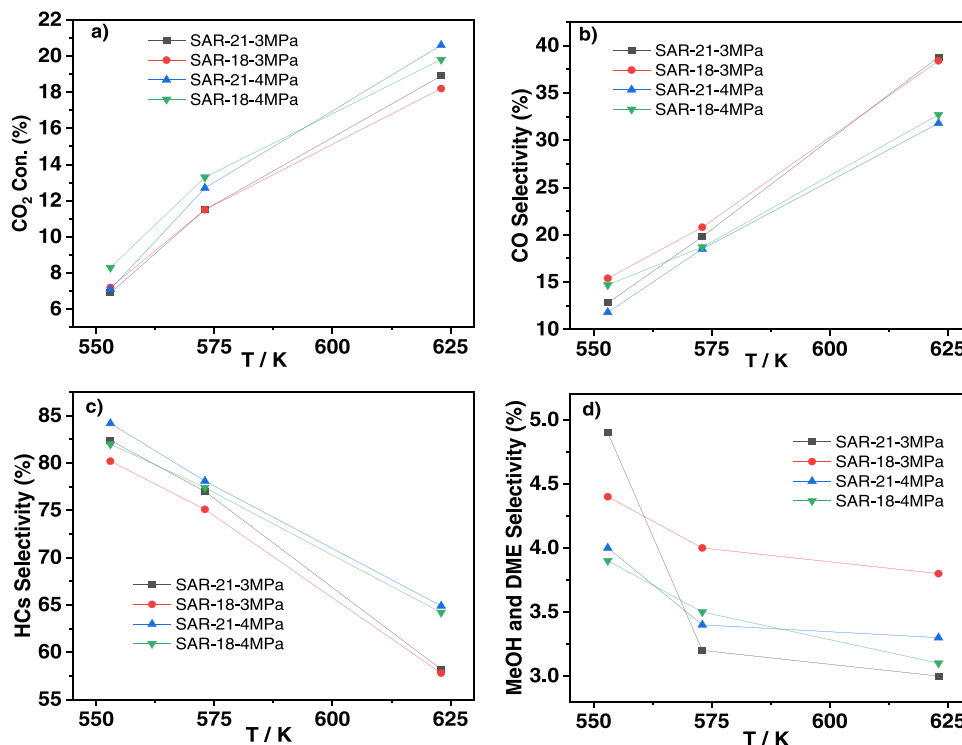

Fig. 10. Catalytic performance of In_2O_3-ZrO_2/desilicated-HZSM-5 (Configuration C, with SAR = 21 & SAR = 18) at various temperatures and pressure at 3.0 and 4.0 MPa: (a) CO_2 conversion (b) CO selectivity (c) Hydrocarbons selectivity and (d) Methanol and DME selectivity.

where the pristine HZSM-5 was replaced by the desilicated-HZSM-5 in the composite catalysts. When the desilicated-HZSM-5 (SAR = 21) was mixed with In_2O_3-ZrO_2, the CO_2 conversion was 7.1% with 84.2% HCs selectivity at 553 K (Fig. 10). When the temperature increased from 553 K to 623 K, the CO_2 conversion and the HCs selectivity were found to be 20.6% and 64.9% at 4.0 MPa, respectively. The results were only slightly different when desilicated HZSM-5 (SAR = 18) was mixed with In_2O_3-ZrO_2. The CO_2 conversion was 8.3% with 82.0% HCs selectivity at 553 K which changed to 19.8% and 64.2% respectively at 623 K. The results in Fig. 10 show that the difference in catalytic performance between the two C configurations with SAR = 21 and SAR = 18 is very small, which is expected since the SAR is similar. However, it should be noted that even though the samples exhibited similar SAR there are differences in acid strength as seen in NH_3 TPD (Fig. 4). In addition, the pore volume is significantly larger for SAR = 18 (Table 1). These differences did not cause any large effect on the CO_2 conversion, CO formation and overall HCs yield, but they influenced the distribution of different HCs species, which will be discussed in a later paragraph.

At 553 K, the C_{5+} selectivity was higher in the case of configuration A having SAR = 59 than SAR = 24. The C_{5+} selectivity decreased when temperature increased from 553 to 623 K over both SAR (Fig. S3e and S4e). The CO selectivity was 15.5% over SAR = 59 whereas it was 13.1% in the case of SAR = 24 (Fig. 9c and S4d). Lower C_{5+} selectivity over SAR = 24 and decreasing C_{5+} with increasing temperature could be caused by more cracking reactions over strong acid sites, which are present with greater concentration over the SAR = 24, based on the NH_3-TPD measurements (Table 1). The C_{5+} selectivity was found to be 65.3% and 42.3% at 553 K and 623 K, respectively over Configuration C with SAR = 21 (Fig. 9a & S3e), while it was 67.2% at 553 K and 46.6% at 623 K with SAR = 18 (Fig. 9c & S4e). The C_{5+} selectivity among HCs over configuration C was slightly higher than configuration A in the case of both sets of HZSM-5 samples over all temperatures (Fig. 9(a & c) & Figs. S3 & S4). It can be stated that the selectivity of C_{5+} also improved when desilicated-HZSM-5 was used instead of pristine HZSM-5. It can be presumed here that the increased mesoporosity of the desilicated samples, as indicated by the N_2 adsorption measurements, reduced the diffusion resistance for larger HCs products.

The C_{5+} selectivity was found to be highest over configuration B compared to A and C at 553 K (Fig. 9a & c). At 553 K, the selectivity of C_{5+} was 70.3% at 4.0 MPa while it was 68.0% at 3.0 MPa K for configuration B with SAR = 21 (Fig. 9a & c). Moreover, the distribution of HCs in the C_5-C_{12} fraction was examined (Fig. 9b & d) and it was observed that the fraction of C_8-C_{12} selectivity among C_5-C_{12} products was higher using configuration B. At 3.0 MPa, the selectivity of C_8-C_{12} increased up to 35.2% at 553 K over configuration B having SAR = 21 while it was 28.1% over configuration A having SAR = 24 (Fig. 9b). Further, the selectivity of C_8-C_{12} reached up to 42.4% at 4.0 MPa over configuration B having SAR = 21 (Fig. 9d). For this case, which exhibited the best performance, the selectivity of C_5-C_8 (gasoline range) was 29.9% and C_{9+} selectivity was 38.1%. However, the selectivity of C_8-C_{12} among C_{5+} products over configuration C was less than configuration A when HZSM-5 with SAR = 24 and SAR = 21 were used. Thus it is clear that the intended oligomerization increased the larger hydrocarbons, which is resulting in that configuration B was the best. However, the beneficial effect of oligomerization using configuration B forming larger amount of C_8-C_{12} was not observed at higher temperatures or when using the HZSM-5 with SAR = 59 and SAR = 18 (data not shown). Thus, the process is very sensitive to catalyst composition and reaction conditions. In the case of HZSM-5 with SAR = 59 and SAR = 18, the selectivity of C_8-C_{12} was similar for configuration A and C. These differences could be due to secondary reactions over strong acid sites which are present in consistently higher concentrations over the SAR = 24 and 21 zeolites compared to their SAR = 59 and 18 counterparts.

The selectivities for HCs could also be influenced by the diffusion properties of the zeolites which is important for the number of carbons and shape of HC chains in longer hydrocarbons. The overall C_{5+} selectivity was higher on desilicated-HZSM-5 (SAR = 18) than desilicated-HZSM-5 (SAR = 21) while the fraction of C_8-C_{12} selectivity was higher over desilicated-HZSM-5 (SAR = 21) than desilicated-HZSM-5 (SAR = 18). There are various factors that could affect the distribution of HCs over zeolites [53], such as acid site density and diffusion effects. Desilicated-HZSM-5 (SAR = 18), exhibit a greater pore size and mesoporosity (see Table 1) with lower acidity and an increased selectivity for C_{5+} products (Fig. S4, SI). We hypothesize that the larger pores could give more aromatic compounds and thereby explain the larger C_{5+} content and lower C_8-C_{12} selectivity for desilicated-HZSM-5 (SAR = 18). Overall, it suggests that a controlled desilication can be used to control the selectivity for desired products. In addition, for oligomerization it is more important to retain acid sites rather than create more mesoporosity.

To summarize, it was observed that methanol selectivity was found to be higher at lower temperatures and higher pressure. Higher methanol selectivity gave higher selectivity for HCs at lower temperatures and higher pressure (Fig. 8 & 10). Thus, the presence of more hydrocarbons leads to more oligomerization reactions over the strong acid sites of HZSM-5. It is suggested that low temperature and high pressure are beneficial for the oligomerization since it was higher at 553 K and 4.0 MPa and not observed at higher temperatures. These results are in line with the study by Wang et. al.[54] who observed a lower yield of liquid hydrocarbons at higher temperatures where the formation of liquid hydrocarbon was due to secondary reactions like oligomerization of ethylene. In addition, the RWGS is an endothermic reaction thus the CO selectivity increased with increasing temperature while it decreased with increasing pressure during the experiments under all configurations (Fig. 8 & 10). It was observed in all configurations that the CH_4 selectivity increased with increasing pressure and temperature among the selectivity for HCs. The methanol and DME selectivities were slightly less in configuration B than in configuration A and C, which could be due to the conversion of unreacted methanol to HCs over the acidic sites of the desilicated HZSM-5 of the second bed.

Configuration B where HZSM-5 with SAR = 24 and SAR = 21 were used, gave higher selectivity for longer HCs. Thus, spent In_2O_3-ZrO_2/HZSM-5 (SAR = 24) and spent desilicated-HZSM-5 (SAR = 21) were chosen for stability test of the catalysts. The spent catalysts were characterized using XRD, N_2 physisorption, and TGA analysis. The crystalline nature was found to be preserved in the spent In_2O_3-ZrO_2/HZSM-5 (SAR = 24) and spent desilicated-HZSM-5 (SAR = 21) (SI, Fig. S5a &b). The sharp peaks in XRD around 2θ = 35 and 65 in spent In_2O_3-ZrO_2/HZSM-5 (SAR = 24) are related to SiC which was used for the packing of the reactor. The mesoporosity and ordered framework were sustained in the spent HZSM-5 (SAR = 21). The specific surface area decreased by 9%. (Fig. S5c, SI and Table 1), which could be due to coke formation. Moreover, the external surface area of the spent catalyst was larger than that of the fresh catalyst, which agreed with data reported in the literature [55]. During the reaction, coke can be deposited both in the internal pore (micro and meso) and on the external surface of the zeolite. The internal coke could cause a decrease in the micropore volume and have a strong impact on the deactivation, whereas the external coke usually has a porous permissible structure allowing the diffusion of the reactants and products and consequently the formation of external coke had less effect on the catalytic performance. Interestingly, Wan et al. [55] observed that the external coke (after being isolated) was a mesoporous material and accounted for an increase in the external surface area as well as the mesoporous volume. It should be noted that the spent sample was dark in color even after the degas step before the N_2 physisorption measurement, which suggests coke formation.

Surprisingly, the TGA analysis (SI, Fig. S5d) showed that the weight loss in the spent desilicated-HZSM-5 was less compared to the fresh desilicated HZSM-5 in the temperature range of 400–670 K. These results suggest that it is more water present in the fresh catalyst. It is possible that coke in the pores of HZSM-5 suppressed the catalyst's ability to absorb water.

4. Conclusions

Direct catalytic hydrogenation of CO_2 to hydrocarbons in a single step is a very interesting process because two steps are interacting, that is the methanol formation (CO_2 -> CH_3OH) and the production of the hydrocarbons (CH_3OH -> hydrocarbon). This study focused on converting CO_2 to fuels where the aim was to increase the yield of liquid-range hydrocarbons (C_{5+}) and especially the longer hydrocarbons in the range C_8-C_{12}. The CO_2 to methanol reaction was catalyzed over an In_2O_3-ZrO_2 catalyst and combined with the zeolite HZSM-5 to further convert the methanol to hydrocarbons. Further, a novel two-bed catalytic configuration was developed to increase the selectivity of liquid-range hydrocarbons (C_{5+}). In the two bed configurations, the first bed contained a bifunctional In_2O_3-ZrO_2/HZSM-5 catalyst and downstream was a second bed of oligomerization catalyst. As an oligomerization catalyst, HZSM-5 was desilicated and characterized using various analytical techniques. To check the effect of SAR and desilication, a comparative study between HZSM-5 with SAR = 24 and HZSM-5 with SAR = 59 was carried out. The oligomerization catalyst polymerizes small hydrocarbons into longer hydrocarbons. The best reaction condition was observed at 553 K, 4.0 MPa with a feed gas ratio of H_2: CO_2 = 3:1, where the CO_2 conversion was 7.2%, the CO selectivity was 11% and the hydrocarbon selectivity was 86% over configuration B where SAR = 24 and SAR = 21 were used with In_2O_3-ZrO_2. For the formed hydrocarbons, the C_{5+} selectivity was 68% and the selectivity for C_8-C_{12} was 42.4%. The two-bed configuration could successfully increase the selectivity for C_{8-12} hydrocarbon products from 29.2% to 42.4% for this specific condition. The increments in C_{8-12} hydrocarbon products were achieved with a milder desilication of the HZSM-5 with SAR = 24 as it contained a higher density of acid sites along with a higher pore volume and average pore size.

CRediT authorship contribution statement

Poonam Sharma: Conceptualization, Data curation, Investigation, Writing – original draft preparation, **Phuoc Hoang Ho:** Data curation, Investigation, Writing – review & editing. **Wei Di:** Investigation, Writing – review & editing. **Derek Creaser:** Conceptualization, Supervision, Writing – review & editing. **Louise Olsson:** Conceptualization, Supervision, Writing – review & editing, Funding acquisition.

Declaration of Competing Interest

The authors declare that they have no known competing financial interests or personal relationships that could have appeared to influence the work reported in this paper.

Data Availability

Data will be made available on request.

Appendix A. Supporting information

Supplementary data associated with this article can be found in the online version at doi:10.1016/j.jcou.2023.102549.

References

[1] H.-J. Ho, A. Iizuka, E. Shibata, Carbon capture and utilization technology without carbon dioxide purification and pressurization: a review on its necessity and available technologies, Ind. Eng. Chem. Res. 58 (2019) 8941–8954.

[2] I. Ghiat, T. Al-Ansari, A review of carbon capture and utilisation as a CO_2 abatement opportunity within the EWF nexus, J. CO_2 Util. 45 (2021), 101432.

[3] A.I. Osman, M. Hefny, M.A. Maksoud, A.M. Elgarahy, D.W. Rooney, Recent advances in carbon capture storage and utilisation technologies: a review, Environ. Chem. Lett. (2020) 1–53.

[4] W. Cho, H. Yu, Y. Mo, CO_2 conversion to chemicals and fuel for carbon utilization, Recent Adv. Carbon Capture Storage (2017) 193.

[5] M. Aresta, Carbon Dioxide as Chemical Feedstock, Wiley Online Library, 2010.

[6] A. Dibenedetto, A. Angelini, P. Stufano, Use of carbon dioxide as feedstock for chemicals and fuels: homogeneous and heterogeneous catalysis, J. Chem. Technol. Biotechnol. 89 (2014) 334–353.

[7] J.H. Edwards, Potential sources of CO_2 and the options for its large-scale utilisation now and in the future, Catal. Today 23 (1995) 59–66.

[8] S. Fuss, W.F. Lamb, M.W. Callaghan, J. Hilaire, F. Creutzig, T. Amann, T. Beringer, W. de Oliveira Garcia, J. Hartmann, T. Khanna, Negative emissions—Part 2: Costs, potentials and side effects, Environ. Res. Lett. 13 (2018), 063002.

[9] S. Das, J. Pérez-Ramírez, J. Gong, N. Dewangan, K. Hidajat, B.C. Gates, S. Kawi, Core–shell structured catalysts for thermocatalytic, photocatalytic, and electrocatalytic conversion of CO_2, Chem. Soc. Rev. 49 (2020) 2937–3004.

[10] A. Mustafa, B.G. Lougou, Y. Shuai, Z. Wang, H. Tan, Current technology development for CO_2 utilization into solar fuels and chemicals: A review, J. Energy Chem. 49 (2020) 96–123.

[11] J. Rogelj, M. Den Elzen, N. Höhne, T. Fransen, H. Fekete, H. Winkler, R. Schaeffer, F. Sha, K. Riahi, M. Meinshausen, Paris Agreement climate proposals need a boost to keep warming well below 2 C, Nature 534 (2016) 631–639.

[12] S.J. Davis, K. Caldeira, H.D. Matthews, Future CO_2 emissions and climate change from existing energy infrastructure, Science 329 (2010) 1330–1333.

[13] G.A. Olah, G.S. Prakash, A. Goeppert, Anthropogenic chemical carbon cycle for a sustainable future, J. Am. Chem. Soc. 133 (2011) 12881–12898.

[14] P.H. Dixneuf, A bridge from CO 2 to methanol, Nat. Chem. 3 (2011) 578–579.

[15] M.Z. Rahman, M.G. Kibria, C.B. Mullins, Metal-free photocatalysts for hydrogen evolution, Chem. Soc. Rev. 49 (2020) 1887–1931.

[16] S.E. Hosseini, M.A. Wahid, Hydrogen production from renewable and sustainable energy resources: promising green energy carrier for clean development, Renew. Sustain. Energy Rev. 57 (2016) 850–866.

[17] S. Sorrell, J. Speirs, R. Bentley, A. Brandt, R. Miller, Global oil depletion: A review of the evidence, Energy Policy 38 (2010) 5290–5295.

[18] R.L. Hirsch, Mitigation of maximum world oil production: Shortage scenarios, Energy Policy 36 (2008) 881–889.

[19] P. Sharma, J. Sebastian, S. Ghosh, D. Creaser, L. Olsson, Recent advances in hydrogenation of CO_2 into hydrocarbons via methanol intermediate over heterogeneous catalysts, Catal. Sci. Technol. (2021).

[20] H. Jahangiri, J. Bennett, P. Mahjoubi, K. Wilson, S. Gu, A review of advanced catalyst development for Fischer–Tropsch synthesis of hydrocarbons from biomass derived syn-gas, Catal. Sci. Technol. 4 (2014) 2210–2229.

[21] G.P. Van Der Laan, A. Beenackers, Kinetics and selectivity of the Fischer–Tropsch synthesis: a literature review, Catal. Rev. 41 (1999) 255–318.

[22] P. Gao, S. Dang, S. Li, X. Bu, Z. Liu, M. Qiu, C. Yang, H. Wang, L. Zhong, Y. Han, Direct production of lower olefins from CO2conversion via bifunctional catalysis, ACS Catal. 8 (2018) 571–578.

[23] K. Fujimoto, T. Shikada, Selective synthesis of C2-C5 hydrocarbons from carbon dioxide utilizing a hybrid catalyst composed of a methanol synthesis catalyst and zeolite, Appl. Catal. 31 (1987) 13–23.

[24] H. Yang, C. Zhang, P. Gao, H. Wang, X. Li, L. Zhong, W. Wei, Y. Sun, A review of the catalytic hydrogenation of carbon dioxide into value-added hydrocarbons, Catal. Sci. Technol. 7 (2017) 4580–4598.

[25] O. Martin, A.J. Martín, C. Mondelli, S. Mitchell, T.F. Segawa, R. Hauert, C. Drouilly, D. Curulla-Ferré, J. Pérez-Ramírez, Indium oxide as a superior catalyst for methanol synthesis by CO_2 hydrogenation, Angew. Chem. Int. Ed. 55 (2016) 6261–6265.

[26] P. Gao, S. Li, X. Bu, S. Dang, Z. Liu, H. Wang, L. Zhong, M. Qiu, C. Yang, J. Cai, Direct conversion of CO 2 into liquid fuels with high selectivity over a bifunctional catalyst, Nat. Chem. 9 (2017) 1019–1024.

[27] E.M. Johansson, Controlling the Pore Size and Morphology of Mesoporous Silica, Linköping University Electronic Press, 2010.

[28] G. Hemighaus, T. Boval, J. Bacha, F. Barnes, M. Franklin, L. Gibbs, N. Hogue, J. Jones, D. Lesnini, J. Lind, Aviation fuels technical review, Chevron Corp. (2006).

[29] F. Jin, P. Zhang, G. Wu, Fundamental kinetics model of acidity-activity relation for ethylene oligomerization and aromatization over ZSM-5 zeolites, Chem. Eng. Sci. 229 (2021), 116144.

[30] S. Miller, Olefin oligomerization over high silica zeolites, Stud. Surf. Sci. Catal. (1988) 187–197.

[31] B.E. Langner, Reactions of olefins on zeolites: The change of the product distribution with time on stream in the reaction of butene-1 on calcined NaNH4-Y, J. Catal. 65 (1980) 416–427.

[32] S.M. Hassan, G. Panchenkov, O. Kuznetsov, Studies on the mechanism and kinetics of propylene oligomerization and hydrooligomerization on zeolites, Bull. Chem. Soc. Jpn. 50 (1977) 2597–2601.

[33] S. Moon, H.-J. Chae, M.B. Park, Oligomerization of light olefins over ZSM-5 and beta zeolite catalysts by modifying textural properties, Appl. Catal. A: Gen. 553 (2018) 15–23.

[34] J. Groen, L. Peffer, J. Moulijn, J. Pérez-Ramırez, Mesoporosity development in ZSM-5 zeolite upon optimized desilication conditions in alkaline medium, Colloids Surf. A: Physicochem. Eng. Asp. 241 (2004) 53–58.

[35] B. Gil, B. Mokrzycki, Z. Sulikowski, S. Olejniczak, Walas, Desilication of ZSM-5 and ZSM-12 zeolites: Impact on textural, acidic and catalytic properties, Catal. Today 152 (2010) 24–32.

[36] R.J. Quann, L.A. Green, S.A. Tabak, F.J. Krambeck, Chemistry of olefin oligomerization over ZSM-5 catalyst, Ind. Eng. Chem. Res. 27 (1988) 565–570.

[37] W. Monama, E. Mohiuddin, B. Thangaraj, M.M. Mdleleni, D. Key, Oligomerization of lower olefins to fuel range hydrocarbons over texturally enhanced ZSM-5 catalyst, Catal. Today 342 (2020) 167–177.

[38] A. de Klerk, Oligomerization of 1-hexene and 1-octene over solid acid catalysts, Ind. Eng. Chem. Res. 44 (2005) 3887–3893.

[39] P. Sharma, P.H. Ho, J. Shao, D. Creaser, L. Olsson, Role of ZrO2 and CeO2 support on the In2O3 catalyst activity for CO2 hydrogenation, Fuel 331 (2023), 125878.

[40] U. Olsbye, S. Svelle, M. Bjørgen, P. Beato, T.V. Janssens, F. Joensen, S. Bordiga, K. P. Lillerud, Conversion of methanol to hydrocarbons: how zeolite cavity and pore size controls product selectivity, Angew. Chem. Int. Ed. 51 (2012) 5810–5831.

[41] A. Ayeshamariam, M. Kashif, S.M. Raja, S. Sivaranjani, C. Sanjeeviraja, M. Bououdina, Synthesis and characterization of In 2 O 3 nanoparticles, J. Korean Phys. Soc. 64 (2014) 254–262.

[42] W. Li, H. Huang, H. Li, W. Zhang, H. Liu, Facile synthesis of pure monoclinic and tetragonal zirconia nanoparticles and their phase effects on the behavior of supported molybdena catalysts for methanol-selective oxidation, Langmuir 24 (2008) 8358–8366.

[43] M. Thommes, K. Kaneko, A.V. Neimark, J.P. Olivier, F. Rodriguez-Reinoso, J. Rouquerol, K.S. Sing, Physisorption of gases, with special reference to the evaluation of surface area and pore size distribution (IUPAC Technical Report), Pure Appl. Chem. 87 (2015) 1051–1069.

[44] M. Milina, S. Mitchell, Z.D. Trinidad, D. Verboekend, J. Pérez-Ramírez, Decoupling porosity and compositional effects on desilicated ZSM-5 zeolites for optimal alkylation performance, Catal. Sci. Technol. 2 (2012) 759–766.

[45] J.C. Groen, L.A. Peffer, J. Pérez-Ramírez, Pore size determination in modified micro-and mesoporous materials. Pitfalls and limitations in gas adsorption data analysis, Microporous Mesoporous Mater. 60 (2003) 1–17.

[46] T.C. Hoff, D.W. Gardner, R. Thilakaratne, J. Proano-Aviles, R.C. Brown, J.-P. Tessonnier, Elucidating the effect of desilication on aluminum-rich ZSM-5 zeolite and its consequences on biomass catalytic fast pyrolysis, Appl. Catal. A: Gen. 529 (2017) 68–78.

[47] V. Rac, V. Rakić, Z. Miladinović, D. Stošić, A. Auroux, Influence of the desilication process on the acidity of HZSM-5 zeolite, Thermochim. Acta 567 (2013) 73–78.

[48] W. Di, P.H. Ho, A. Achour, O. Pajalic, L. Josefsson, L. Olsson, D. Creaser, CO2 hydrogenation to light olefins using In2O3 and SSZ-13 catalyst− Understanding the role of zeolite acidity in olefin production, J. CO2 Util. 72 (2023), 102512.

[49] C. Cheng, G. Li, D. Ji, Y. Zhao, J. Shen, Regulating hierarchical structure and acidity of HZSM-5 for methanol to aromatics via protective desiliconization and external surface modification, Microporous Mesoporous Mater. 312 (2021), 110784.

[50] S. Abello, A. Bonilla, J. Perez-Ramirez, Mesoporous ZSM-5 zeolite catalysts prepared by desilication with organic hydroxides and comparison with NaOH leaching, Appl. Catal. A: Gen. 364 (2009) 191–198.

[51] D. Rojo-Gama, M. Signorile, F. Bonino, S. Bordiga, U. Olsbye, K.P. Lillerud, P. Beato, S. Svelle, Structure–deactivation relationships in zeolites during the methanol–to-hydrocarbons reaction: Complementary assessments of the coke content, J. Catal. 351 (2017) 33–48.

[52] B. Wang, Zeolite deactivation during hydrocarbon reactions: characterisation of coke precursors and acidity, product distribution Univ. Lond., Univ. Coll. Lond. (U. Kingd.) 2006.

[53] Y. Ji, H. Yang, W. Yan, Strategies to enhance the catalytic performance of ZSM-5 zeolite in hydrocarbon cracking: A review, Catalysts 7 (2017) 367.

[54] K.K. Ramasamy, Y. Wang, Ethanol conversion to hydrocarbons on HZSM-5: Effect of reaction conditions and Si/Al ratio on the product distributions, Catal. Today 237 (2014) 89–99.

[55] Z. Wan, G.K. Li, C. Wang, H. Yang, D. Zhang, Relating coke formation and characteristics to deactivation of ZSM-5 zeolite in methanol to gasoline conversion, Appl. Catal. A: Gen. 549 (2018) 141–151.